

See discussions, stats, and author profiles for this publication at: <https://www.researchgate.net/publication/263981856>

4,4'-Diaminodiphenyl Sulfone Functionalized SBA-15: Toluene Sensing Properties and Improved Proton Conductivity

ARTICLE in THE JOURNAL OF PHYSICAL CHEMISTRY C · JANUARY 2014

Impact Factor: 4.77 · DOI: 10.1021/jp406688c

CITATIONS

8

READS

19

5 AUTHORS, INCLUDING:



Zhiming Duan

Shanghai University

9 PUBLICATIONS 198 CITATIONS

[SEE PROFILE](#)



Qun Xiang

Shanghai University

20 PUBLICATIONS 900 CITATIONS

[SEE PROFILE](#)



Jiaqiang Xu

Shanghai University

141 PUBLICATIONS 3,731 CITATIONS

[SEE PROFILE](#)

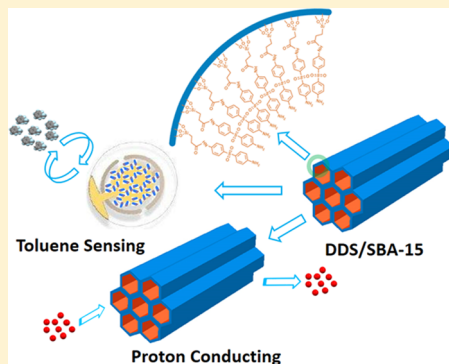
4,4'-Diaminodiphenyl Sulfone Functionalized SBA-15: Toluene Sensing Properties and Improved Proton Conductivity

Nana Qian, Zhiming Duan,* Yongheng Zhu, Qun Xiang, and Jiaqiang Xu*

Department of Chemistry, College of Sciences, Shanghai University, Shanghai, 200444, P. R. China

Supporting Information

ABSTRACT: 4,4'-Diaminodiphenyl sulfone functionalized SBA-15 (DDS/SBA-15) with various loading amounts of DDS has been prepared via a postsynthesis grafting method. The 2D hexagonal mesoporous structures of these hybrids have been confirmed by small-angle X-ray scattering (SAXS), transmission electron microscopy (TEM), and N₂ adsorption–desorption isotherms. The covalent grafting of DDS onto the SBA-15 was further confirmed by Fourier transform infrared spectroscopy (FT-IR). DDS/SBA-15 based quartz crystal microbalance (QCM) sensor shows good selectivity and quick response toward toluene vapor, and the detection limit is down to 20 ppb. Impedance spectroscopy measurements showed that the proton conductivity properties of DDS/SBA-15 depended on the loading amount of DDS. These hybrids demonstrated improved proton conductivities compared with pristine SBA-15, and a highest value of 2.26 × 10⁻⁴ S cm⁻¹ has been observed when the DDS loading amount is 0.37 mmol g⁻¹. Therefore, DDS/SBA-15 could serve as a promising candidate for both volatile organic compound (VOC) vapor sensing and proton conducting materials.



1. INTRODUCTION

Numerous ordered mesoporous silicas have been investigated during the past few decades.^{1–5} Among them, SBA-15 appears to be more attractive and potentially useful for gas storage and separations,^{6–8} sensors,^{9–12} catalysis,^{13–15} and drug delivery^{16–18} due to its high surface areas, ordered pore systems, and well-defined pore radius distributions. Significant efforts have been made to functionalize SBA-15 with various groups for tuning or improving their desired properties and selectivities.^{19,20} The functionalization on the surfaces of SBA-15 is usually achieved through two general methods namely by postsynthesis grafting^{21–28} or by co-condensation.^{29–33} The main advantage of the latter had been described as the even distribution of the functional groups throughout the entire material, while the grafted material retained greater hydrothermal stability compared with the co-condensed one. Furthermore, postsynthesis grafting is a facile and economic way to introduce different functional groups onto the wall of SBA-15. Based on the above considerations, we have successfully demonstrated a nerve agent dimethyl methylphosphonate (DMMP) sensor based on fluoroalcohol or fluorinated-phenol derivatives functionalized SBA-15 hybrids.¹¹ The promising application of mesoporous materials in the current energy and environmental issues encourages us extend our research to other interesting functional groups.

Toluene as one of the most important volatile organic compounds (VOC), widely used in industry and interior decoration, may bring about serious medical, environmental, and explosion dangers.^{34,35} The development of chemical sensors capable of monitoring toluene at the parts per million

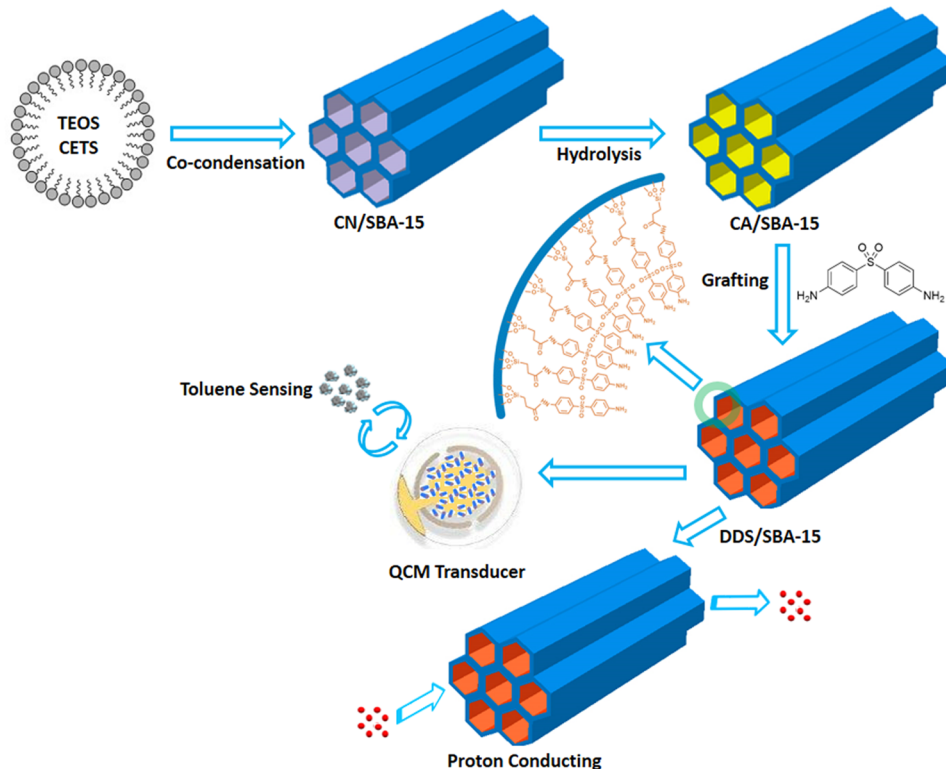
level has attracted widespread interest.³⁶ Amino modified styrene copolymers have shown good toluene sensing properties by using a quartz crystal microbalance (QCM) technique.³⁷ Proton transfer in aqueous media is an extremely widespread and important process in nature and technology.^{38,39} Sulfonic acid-functionalized mesoporous electrolytes with high proton conductivity under dry conditions were reported recently,⁴⁰ and the well-known polysulfone backbone in polymers had also been explored for high proton conductivity applications.^{41,42} Systematic works on functionalization of Si-MCM-41 with SO₃H-groups have been reported, and the hybrid materials exhibit a very high proton conductivity of up to 0.2 S/cm at 100% relative humidity. Functionalization of Si-MCM-41 with SO₃H-groups by a co-condensation method exhibits a very homogeneous distribution of the SO₃H-groups along the channels and explaining the observed higher proton conductivities compared to grafted samples.^{43–45} SBA-15 with large porosities and silanol groups provides possible interfaces for both gas diffusion and proton conduction. It could be an ideal candidate for VOC vapor sensing and proton conducting materials after appropriate grafting of functional groups. 4,4'-Diaminodiphenyl sulfone (DDS) possessing electron-poor diphenyl sulfone unit and electron-releasing *p*-amino substituents could act as a binary functional group for VOC vapor sensing and proton conducting of SBA-15.⁴⁶ Presumably, when DDS was incorporated into the backbone of SBA-15, the

Received: July 7, 2013

Revised: January 6, 2014

Published: January 8, 2014



Scheme 1. Synthesis of DDS Functionalized Mesoporous Silica, Their Toluene Sensing, and Proton Conducting Behaviors^a

^aTEOS, tetraethylorthosilicate; CETS, 2-cyanoethyltriethoxysilane; CN/SBA-15, cyanide ($-CN$) functionalized SBA-15; CA/SBA-15, carboxylate ($-COOH$) functionalized SBA-15; DDS/SBA-15, 4,4'-diaminodiphenyl sulfone (DDS) functionalized SBA-15.

existence of phenyl groups may provide a combination of both hydrophobic effects and intermolecular interactions for improvement of selectivity in VOC vapor sensing. Furthermore, the ordered 1D straight channel and larger pore size of SBA-15 facilitate the diffusion and enhance the accessibility of water, and the hydrophilic silanol group, amino group, and sulfonyl group would act as carriers or pathway for the proton conduction.

In the present study, we report a synthetic strategy for DDS functionalized SBA-15 with various loading amounts of DDS via a postsynthesis grafting method. We have fully characterized the 2D hexagonal mesoporous structures of these hybrids by small-angle X-ray scattering (SAXS), transmission electron microscopy (TEM), and N_2 adsorption–desorption measurements. Using these mesoporous hybrids, we have fabricated quartz crystal microbalances (QCM) transducer showing good sensitivity, selectivity, and short response time toward toluene vapor. Furthermore, we report the preliminary results of proton conductivity at ambient temperature under wet conditions based on our hybrids, and they demonstrate improved proton conductivities compared with pristine SBA-15 at 100% RH. A highest conductivity of $2.26 \times 10^{-4} \text{ S cm}^{-1}$ with the DDS loading amount of 0.37 mmol g^{-1} has been observed. Therefore, our DDS functionalized SBA-15 could serve as a promising candidate for both VOC vapor sensing and proton conducting materials.

2. EXPERIMENTAL SECTION

The representative route was depicted in Scheme 1.

2.1. Materials. All reagents were commercially available and used as received: the triblock copolymer pluronic P123 (EO_{20}

$PO_{70}EO_{20}$, $M_w = 5800$) (Aldrich), and 2-cyanoethyltriethoxysilane (CETS) (Alfa Aesar, 97%); tetraethylorthosilicate (TEOS) (SCRC, 28.4%), 4,4'-diaminodiphenyl sulfone (DDS) (SCRC, 98.0%), N-ethyl-N'-(3-dimethylaminopropyl) carbodiimide hydrochloride (Aladdin, 98.5%), and 1-hydroxybenzotriazole (Energy Chemical, 99%).

2.2. Synthesis. **2.2.1. Synthesis of Carboxylate ($-COOH$) Functionalized SBA-15 (CA/SBA-15).** CA/SBA-15 was prepared according to the literature method involving a one-pot synthesis of cyanide ($-CN$) functionalized SBA-15 (CN/SBA-15) followed by treatment with sulfuric acid.^{47,48} Typically, the synthesis of CN/SBA-15 started from the premixing of a hydrochloric acid solution of the triblock copolymer Pluronic P123 and CETS. The mixture was stirred up to 30 min and then followed by slow addition of tetraethylorthosilicate (TEOS). The molar composition of the mixture was chosen according to the reported ratio, that is, x TEOS: $(1 - x)$ CETS: 5.9 HCl: 193 H_2O : 0.017 P123, where $x = 0.1\text{--}0.5$. The mixture was stirred at 38°C for 24 h followed by hydrothermal aging at 80°C without stirring for 24 h. The product was filtered, washed, and dried.

As-synthesized CN/SBA-15 was converted to CA/SBA-15 by removing of the template and hydrolysis of the $-CN$ groups. Redispersed sample of CN/SBA-15 in 48 wt % H_2SO_4 solution was stirred and heated at 90°C for 24 h. The solid was collected and well-washed and then vacuum-dried at 60°C overnight.

2.2.2. Synthesis of 4,4'-Diaminodiphenyl Sulfone (DDS) Functionalized SBA-15 (DDS/SBA-15). DDS/SBA-15 was obtained by amidation reaction between DDS and CA/SBA-15.^{11,49} A typical procedure was given as follows: 0.05 g of as-

synthesized CA/SBA-15 was introduced into a tetrahydrofuran (THF) solution of DDS. The mixture was stirred at 0 °C for 2 h, then NaOH (0.01 g, 2.4 mmol), N-ethyl-N'-(3-dimethylaminopropyl) carbodiimide hydrochloride (0.27 g, 1.4 mmol), and 1-hydroxybenzotriazole (0.02 g, 1.4 mmol) were added. After another 2 h at 0 °C, the reaction was conducted at r.t. for 24 h. The resulting solid was filtered, washed thoroughly with acetonitrile and deionized water, and vacuum-dried at 70 °C overnight.

DDS/SBA-15 samples with different loading amounts of DDS were obtained by varying the amount of DDS added to the reaction. The loading amount was estimated by CHN elemental analysis. DDS/SBA-15-1, DDS/SBA-15-2, and DDS/SBA-15-3 correspond to the samples with loading amount of 0.12, 0.23, and 0.37 mmol g⁻¹, respectively.

2.3. Physical Characterization. The pore structure of the hybrids was characterized by small-angle X-ray scattering (SAXS), transmission electron microscopy (TEM), and N₂ adsorption–desorption measurements. SAXS patterns were recorded at Shanghai Synchrotron Radiation Facility (SSRF) on beamline BL16B1 ($\lambda = 1.24 \text{ \AA}$, $D_x = 1.6 \text{ m}$). TEM measurements were taken on a JEOL JEM-2010F field emission electron microscope with an acceleration voltage of 120 kV. N₂ adsorption–desorption isotherms were measured at 77 K using a Micromeritics ASAP 2020 system. In all cases, samples were vacuum degassed at 100 °C for 24 h before adsorption–desorption measurements. Specific surface area was calculated by the Brunauer, Emmett, and Teller (BET) method⁵⁰ from the adsorption branches in the relative pressure range of 0.05–0.25, and the total pore volume was evaluated at a relative pressure of 0.95. Pore size distributions were evaluated using the Barrett–Joyner–Halenda (BJH) method⁵¹ from the desorption branches of the nitrogen isotherms. The FTIR spectra were obtained by the KBr pellet method on a Nicolet Avatar 370.

2.4. Fabrication of Quartz Crystal Microbalances (QCM) Sensors and QCM Adsorption Measurements. QCM adsorption measurements were performed on a modified setup we had reported previously.^{11,52} QCM resonators coated with silver electrodes were purchased from Chenjing Electronic Co., China. The resonance frequency was 10⁷ Hz (AT-cut), and the decrease in frequency ($-\Delta F$) is proportionate with an increase in mass (Δm) according to the Sauerbrey equation ($\Delta F = -2.26 \times 10^{-6} f^2 \Delta m / A$).⁵³ The QCM sensors were obtained by the following procedure: the water/ethanol dispersion of as-synthesized hybrid materials was drop-casted onto a QCM electrode, and as-made sensors were dried in an infrared box for the evaporation of solvents. QCM chips were vertically suspended inside a sealed chamber with gas inlet/outlet, in which nitrogen was used as carrier gas. All measurements were conducted at 25 °C in an air-conditioned room. In a typical measurement, the QCM sensor was flushed with nitrogen stream until a stable baseline was obtained; then the analyte vapor was introduced by injection. A stable response to analyte would be obtained after several minutes. At the end of each cycle, nitrogen stream was reintroduced into the chamber to re-establish the baseline.

2.5. Proton Conductivity Measurements of the As-Synthesized Organic–Inorganic Hybrids. Proton conductivities were measured using the impedance method on pressed pellets (~0.5–1.5 mm thickness × 4–5 mm ϕ). The impedance measurements were carried out by a conventional quasi-four-probe method at r.t. on a RTS-8 Corrosion Electrochemical System. Prior to the measurement, the pellets

were inserted into a humidification chamber with a relative humidity of 100% for 48 h. Proton conductivity was calculated from Nyquist impedance plots⁵⁴ by the following equation: $\sigma = L/(RA)$, where σ is the proton conductivity, L is the thickness of the pellet, R is the resistance of the pellet, and A is the area of the pellet.

3. RESULTS AND DISCUSSION

3.1. Characterization of Pristine and DDS Functionalized SBA-15. SAXS patterns (Figure 1a), N₂ adsorption–desorption isotherms (Figure 1b), pore size distribution (Figure 1c), and TEM images (Figure 2) of as-synthesized pristine and DDS functionalized SBA-15 samples indicate typical characteristics of well-defined and aligned 2D hexagonal mesostructures. The properties derived from SAXS and N₂ adsorption–desorption isotherms were summarized in Table 1.

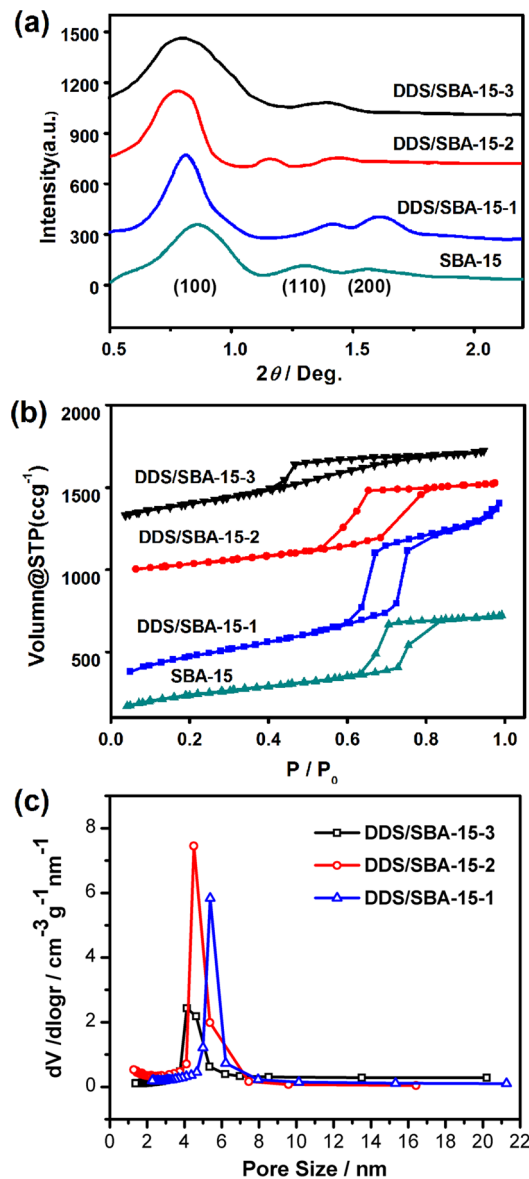


Figure 1. (a) Small angle X-ray scattering patterns and intensities of SBA-15-1 to 3, which were offset by 300, 700, and 1020 au for clarity; (b) N₂ adsorption–desorption isotherms and isotherms of SBA-15-1 to 3, which were offset by 300, 730, and 1270 cm³/g STP for clarity; (c) pore size distributions of DDS functionalized mesoporous silica.

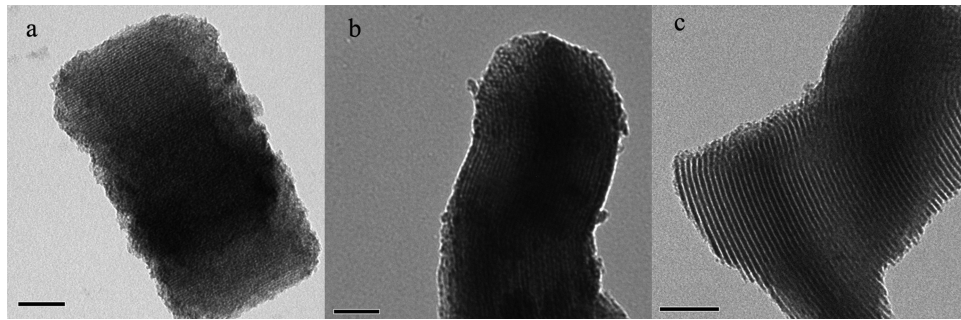


Figure 2. TEM images of DDS functionalized mesoporous silica: (a) DDS/SBA-15-1, (b) DDS/SBA-15-2, (c) DDS/SBA-15-3. Note: Scale bar = 100 nm.

Table 1. Textural Data and Loading Amount of DDS-Functionalized Mesoporous Silica^a

sample	S_{BET} ($\text{m}^2 \text{ g}^{-1}$)	V_T ($\text{cm}^3 \text{ g}^{-1}$)	D_p (nm)	a_0 (nm)	t_{wall} (nm)	DDS (mmol g^{-1})
SBA-15	852	1.11	6.2	10.3	4.1	
DDS/SBA-15-1	486	0.77	5.4	9.7	4.3	0.12
DDS/SBA-15-2	414	0.73	4.9	9.7	4.8	0.23
DDS/SBA-15-3	312	0.68	4.7	11.1	6.4	0.37

^a S_{BET} is the surface area determined by the BET method between the relative pressures (P/P_0) 0.06–0.26. V_T is the total pore volume obtained using the t -plot method. The total pore volume was estimated from the amount of N_2 adsorbed at a relative pressure of 0.95. D_p is the pore diameter calculated by means of the BJH method from the desorption branch of the isotherm. d_{100} is the SAXS spacing of the (100) reflection of a 2D-hexagonal (P 6 mm) plane array of pores. a_0 is the unit cell parameter calculated by SAXS, where $a_0 = 2 d_{100}/\sqrt{3}$. t_{wall} is the wall thickness calculated using the equation $t_{\text{wall}} = a_0 - D_p$. The loading amount of DDS is estimated by elemental analysis.

The SAXS patterns of pristine and DDS functionalized SBA-15 samples showed strong diffraction peaks in the range of $2\theta = 0.5\text{--}1.0^\circ$ and weak peaks in the range of $2\theta = 1.0\text{--}2.0^\circ$. These peaks are indexed as (100), (110), and (200) planes of the 2D-hexagonal mesopore structure. This result is consistent with the TEM images which also showed a hexagonal mesostructure with one-dimensional short-channels. The peaks indexed as (100) plane of DDS functionalized SBA-15 samples remained, indicating that the 2D-hexagonal mesopore structure of SBA-15 is preserved after carboxylate functionalization and *in situ* amidation reaction.¹¹ However, the decreasing of the peak intensity and the broadening of the peak width suggest the incorporation of DDS reduces the crystallinity of the mesophase.^{55,56}

All of the samples showed type IV-shaped adsorption–desorption isotherms according to the IUPAC classification,⁵⁷ which is a characteristic of mesoporous materials (pore diameters of 2–50 nm). Clear H1-type hysteresis loops at high relative pressure were observed for pristine SBA-15, DDS/SBA-15-1, and DDS/SBA-15-2, suggesting the existence of open-ended cylindrical mesopores in association with capillary condensation and the limiting uptake at high relative pressure. DDS/SBA-15-3 showed H2-type hysteresis loops at high relative pressure, which revealed an intermediate phase between open-ended cylindrical and bottleneck-like mesopore structures. Grafting DDS onto CA/SBA-15 affects the BET specific surface area and porosity of the hybrid, giving additional proof of the inner channel immobilization of DDS. The BET surface area declines from 852 to 312 $\text{m}^2 \text{ g}^{-1}$ as the loading amount of DDS in the silica precursor is increased from pristine SBA-15 to DDS/SBA-15-3. The similar trend was observed for the total pore volume decreasing from 1.11 to 0.68 $\text{cm}^3 \text{ g}^{-1}$, concomitant with the mean pore diameters ranging from 6.2 to 4.7 nm (Figure 1c), and the wall thickness changing from 4.1 to 6.4 nm, respectively (Table 1). The slight change in the lattice constant a_0 of the pore lattice from SBA-15 to DDS/SBA-15-2

may suggest the good preservation of the 2D-hexagonal mesopore structure up to 0.23 mmol g^{-1} loading amount of DDS. The abnormal a_0 of DDS/SBA-15-3 may originate from the intermediate mesopore structure. The NSA value (normalized surface area, NSA, has been introduced to quantify the pore blocking effects and NSA is defined as: $\text{NSA} = [\text{SA}_{\text{DDS/SBA-15}}/(1-y)]/(1/\text{SA}_{\text{Pristine SBA-15}})$, where $\text{SA}_{\text{DDS/SBA-15}}$ and $\text{SA}_{\text{Pristine SBA-15}}$ represent the specific area of DDS grafted SBA-15 and pristine SBA-15, respectively, and y is the weight fraction of DDS in the materials)⁵⁸ of DDS/SBA-15-3 is 0.52, much lower than unity, indicating a possible pore blocking in ink-bottle pores.

The TEM images of DDS/SBA-15-1 to DDS/SBA-15-3 presented in Figure 2a–c exhibit the typical P 6 mm hexagonal morphology with well-ordered 1D arrays. The preservation of the cylindrical shape of the pores and their hexagonal mesostructure indicates the channel structure of parent SBA-15 is not destroyed after grafting of DDS.

The FT-IR spectra reveal the existence of a silica network and grafted DDS as shown in Figure 3. The OH stretching vibrations of the silanol groups (Si-OH) and adsorbed water appear between 3700 and 3000 cm^{-1} . The vibration bands centered at 1080 cm^{-1} , 803 cm^{-1} and 462 cm^{-1} corresponding to the Si–O asymmetric stretching, Si–O symmetric stretching, and Si–O bending further confirm the formation of the dense silica network.⁵⁹ The appearance of characteristic bands including C–H stretching vibration of aliphatic CH_2 (3000 to 2850 cm^{-1}), stretching and bending vibration of $\text{S}=\text{O}$ (1330 and 550 cm^{-1}), and stretching vibration of $-\text{CONH}-$ (1698 to 1541 cm^{-1}) indicate the successful grafting of DDS onto the wall of SBA-15.

3.2. Gas-Sensing Properties of DDS Functionalized SBA-15. Gas-sensing properties of DDS functionalized SBA-15 have been investigated by QCM transducer. The comparison of responses of DDS/SBA-15-3 and pristine SBA-15 based QCM sensor upon exposure to different vapors are shown in Figure 4.

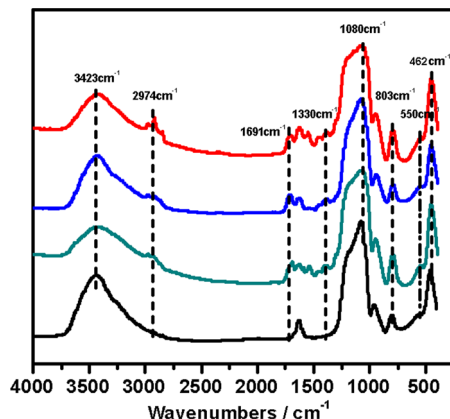


Figure 3. FT-IR spectra of DDS functionalized mesoporous silica. Black, SBA-15; cyan, DDS/SBA-15-1; blue, DDS/SBA-15-2; red, DDS/SBA-15-3.

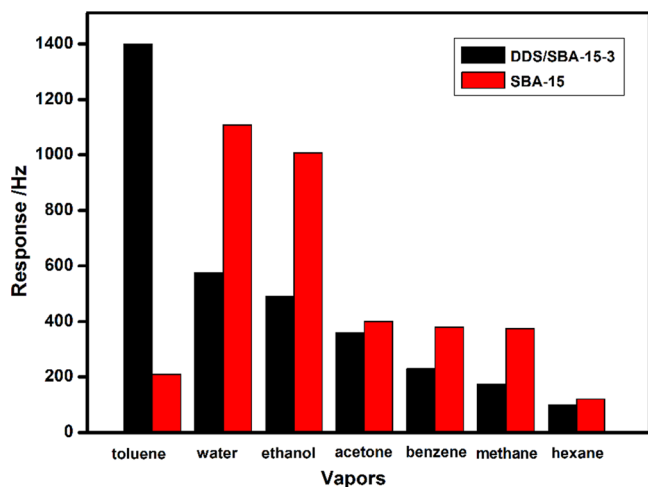


Figure 4. Frequency changes of DDS/SBA-15-3 and SBA-15 based sensors upon exposure to saturated common organic solvents versus 120 ppm toluene vapor at room temperature.

It is obviously seen that DDS/SBA-15-3 based QCM sensor shows a good selectivity to toluene vapor (the toluene uptake capacity of DDS/SBA-15-3 is ca. 4.03 mmol/g at $P/P_0 = 0.95$, see Figure S1 in SI). When QCM sensor exposes to selected vapors (all at 120 ppm), it shows the highest frequency change of 1400 Hz to toluene, and the lowest one (100 Hz) to *n*-hexane. The preferential selectivity toward toluene may indicate the $\sigma-\pi$ interactions of the toluene methyl group with the DDS aromatic phenyl group in combination with the $\pi-\pi$ interactions.⁶⁰ Although the hydroxyl group on the wall of SBA-15 may improve the affinity to some solvents (water and ethanol) able to form hydrogen bonds, the sensitivity toward these solvents has been reduced by the grafting of DDS. Besides, the introduction of amino group into the mesoporous structure may improve the sorption capacity to toluene vapor.³⁷

The responses of DDS/SBA-15-3 based QCM sensor toward toluene vapor are shown in Figure 5a. After a steady frequency had been obtained in the dry N_2 atmosphere, the introduction of 100 ppm toluene vapor leads to a decrease of 1200 Hz in frequency and results in a positive ΔF . The response–recovery cycle was less than 1 min in three successive cycles. High sensitivity and quick response of QCM sensor were further confirmed by successive recording of five response cycles at

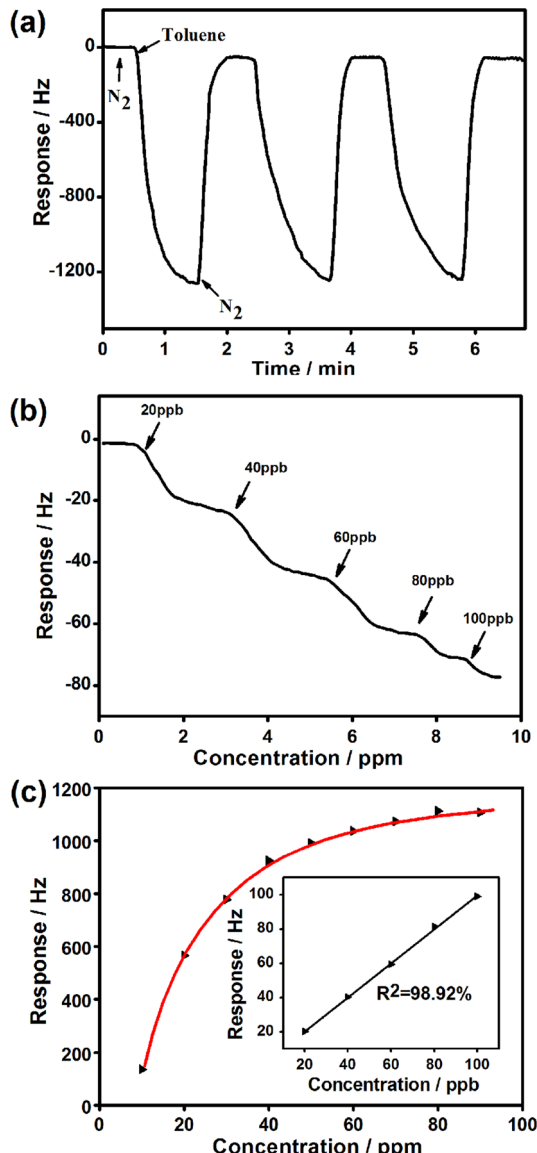


Figure 5. (a) Short-term repeatable and reversible sensing response to 100 ppm of toluene vapor; (b) real-time response curves of the sensor upon exposure to successive increasing concentrations of toluene vapor. (c) Sensing responses versus various concentrations of toluene vapor.

different concentrations of toluene vapor ranging from 20 to 100 ppb (Figure 5b). The sensor shows the lowest detection limit of 20 ppb, and it indicates toluene vapor sensing in parts per billion level. As shown in Figure 5c, the sensor displays a linear response with concentration in the ppb level, while it tends to be saturated with concentration in the ppm level.

3.2. Proton Conductivity of DDS Functionalized SBA-15. The proton conductivities (σ) were examined by an AC impedance method using a pressed pellet of the finely ground powder sample of DDS functionalized SBA-15 with several DDS loading amounts (Figure 6). The σ value of pristine SBA-15 is calculated as $3.32 \times 10^{-5} \text{ S cm}^{-1}$ from the Nyquist plot. When the loading amount is increased, σ increases and reaches a peak value of $2.26 \times 10^{-4} \text{ S cm}^{-1}$ with the loading amount of 0.37 mmol g⁻¹, then decreases with the increase of loading amount. This suggests that the regular structure and typical hexagonal 1D pore channel may benefit the transport of

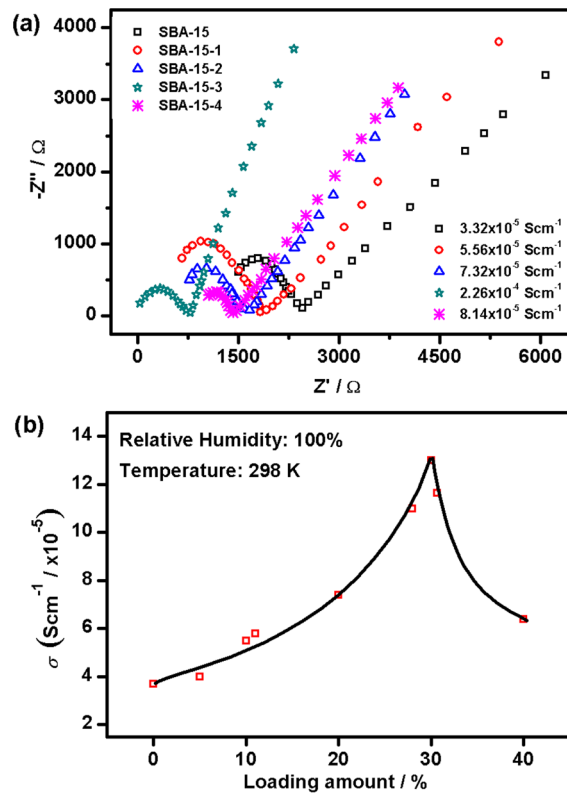


Figure 6. (a) Nyquist plots for proton conductivities of DDS functionalized mesoporous silica at 298 K and RH 100%; (b) curve of proton conductivities with increasing loading amounts of DDS at 298 K and RH 100%.

proton. DDS/SBA-15 is not an anhydrous proton conductor, but it shows moderate proton conductivity under wet conditions which is comparable with many proton conducting MOFs,^{61,62} and obviously lower than sulfonic acid functionalized SBA-15⁴⁰ or MCM-41.^{43,63} Although the origin of the proton conductivity of DDS functionalized SBA-15 is not very clear, we proposed that this conductivity may follow a mixed mechanism including a so-called Grotthus mechanism⁶⁴ and a vehicular mechanism⁶⁵ upon referring to the transport mechanism of sulfonic acid functionalized MCM-41. The former shows that the proton transport is mainly based on hopping of the protons, and the latter indicates that the diffusion of H_3O^+ ions supports the proton transport. In our system, we consider the Grotthus mechanism as a main reason for the proton conducting; however, to a smaller extent, the vehicular mechanism could not be excluded. The polar environment and the channel geometry of the pores, created by the bound water molecules and electronegative sulfonyl group of DDS, could help to keep water, enhance the proton hopping and H_3O^+ ion diffusion, and therefore provide favorable pathways for proton conduction through the tested pellets. Besides, the grafting DDS may rotate and vibrate more easily after the increasing of the temperature; therefore the amino groups and sulfonyl groups could encounter each other more easily and thus facilitate the direct proton transport.

4. CONCLUSIONS

We have obtained DDS functionalized SBA-15 with various loading amounts of DDS, and the measurements of small-angle X-ray scattering (SAXS), transmission electron microscopy

(TEM), and N_2 adsorption–desorption indicate the preservation of 2D hexagonal mesoporous structures after functional grafting. The DDS/SBA-15 based QCM sensor shows a good selectivity and quick response toward toluene vapor due to the combination of $\sigma-\pi$ and $\pi-\pi$ interactions of the toluene with the DDS aromatic phenyl group, and the detection limit is at the parts per billion level. The material exhibits improved proton conductivity with the increase of DDS loading amount compared with pristine SBA-15, and a highest value of $2.26 \times 10^{-4} \text{ S cm}^{-1}$ has been observed with the DDS loading amount of 0.37 mmol g⁻¹. The mechanism of proton transfer in our material may ascribe to a mixed mechanism including Grotthus mechanism and a vehicular mechanism, and a systematic investigation is still on the way. This study may motivate us to engage in detailed exploration of DDS functionalized SBA-15 for practical applications of VOC gas sensing and proton conductivity.

■ ASSOCIATED CONTENT

S Supporting Information

Figure S1: The toluene adsorption–desorption isotherms. This material is available free of charge via the Internet at <http://pubs.acs.org>.

■ AUTHOR INFORMATION

Corresponding Authors

*Phone: +86-21-6613-8002. E-mail: duanzm@shu.edu.cn.

*Phone: +86-21-6613-2701. E-mail: xujiaqiang@shu.edu.cn.

Notes

The authors declare no competing financial interest.

■ ACKNOWLEDGMENTS

The authors are thankful for financial support from National Nature Science Foundation of China (no. 61071040) and National Youth Science Foundation of China (no. 21201118).

■ REFERENCES

- Kresge, C. T.; Leonowicz, M. E.; Roth, W. J.; Vartuli, J. C.; Beck, J. S. Ordered Mesoporous Molecular Sieves Synthesized by A Liquid-Crystal Template Mechanism. *Nature* **1992**, *359*, 710–712.
- Zhao, D.; Huo, Q.; Feng, J.; Chmelka, B. F.; Stucky, G. D. Nonionic Triblock and Star Diblock Copolymer and Oligomeric Surfactant Syntheses of Highly Ordered, Hydrothermally Stable, Mesoporous Silica Structures. *J. Am. Chem. Soc.* **1998**, *120*, 6024–6036.
- Selvam, P.; Bhatia, S. K.; Sonvane, C. G. Recent Advances in Processing and Characterization of Periodic Mesoporous MCM-41 Silicate Molecular Sieves. *Ind. Eng. Chem. Res.* **2001**, *40*, 3237–3261.
- Bonneviot, L.; Beland, F.; Danumah, C.; Giasson, S. *Mesoporous Molecular Sieves: Proceedings of the 1st International Symposium*; Elsevier Science Ltd.: New York, 1998.
- Zhao, D.; Wan, Y.; Zhou, W. *Ordered Mesoporous Materials*; Wiley-VCH Verlag GmbH: Weinheim, 2013.
- Hicks, J. C.; Dreser, J. H.; Fauth, D. J.; Gray, M. L.; Qi, G.; Jones, C. W. Designing Adsorbents for CO_2 Capture from Flue Gas-Hyperbranched Aminosilicas Capable of Capturing CO_2 Reversibly. *J. Am. Chem. Soc.* **2008**, *130*, 2902–2903.
- Sayari, A.; Belmabkhout, Y. Stabilization of Amine-Containing CO_2 Adsorbents: Dramatic Effect of Water Vapor. *J. Am. Chem. Soc.* **2010**, *132*, 6312–6314.
- Wang, L.; Yang, R. T. Increasing Selective CO_2 Adsorption on Amine-Grafted SBA-15 by Increasing Silanol Density. *J. Phys. Chem. C* **2011**, *115*, 21264–21272.
- Zarabadi-Poor, P.; Badiei, A.; Yousefi, A. A.; Barroso-Flores, J. Selective Optical Sensing of $\text{Hg}(\text{II})$ in Aqueous Media by H-Acid/

- SBA-15: A Combined Experimental and Theoretical Study. *J. Phys. Chem. C* **2013**, *117*, 9281–9289.
- (10) Zhu, Y.; Li, H.; Zheng, Q.; Xu, J.; Li, X. Amine-Functionalized SBA-15 with Uniform Morphology and Well-Defined Mesostructure for Highly Sensitive Chemosensors to Detect Formaldehyde Vapor. *Langmuir* **2012**, *28*, 7843–7850.
- (11) Zheng, Q.; Zhu, Y.; Xu, J.; Cheng, Z.; Li, H.; Li, X. Fluoroalcohol and Fluorinated-Phenol Derivatives Functionalized Mesoporous SBA-15 Hybrids: High-Performance Gas Sensing toward Nerve Agent. *J. Mater. Chem.* **2012**, *22*, 2263–2270.
- (12) Lee, H. J.; Park, K. K.; Kupnik, M.; Melosh, N. A.; Khuri-Yakub, B. T. Mesoporous Thin-film on Highly-Sensitive Resonant Chemical Sensor for Relative Humidity and CO₂ Detection. *Anal. Chem.* **2012**, *84*, 3063–3066.
- (13) Villanneau, R.; Marzouk, A.; Wang, Y.; Djamaa, A. B.; Laugel, G.; Proust, A.; Launay, F. Covalent Grafting of Organic-Inorganic Polyoxometalates Hybrids onto Mesoporous SBA-15: A Key Step for New Anchored Homogeneous Catalysts. *Inorg. Chem.* **2013**, *52*, 2958–2965.
- (14) Nakazawa, J.; Smith, B. J.; Stack, T. D. P. Discrete Complexes Immobilized onto Click-SBA-15 Silica: Controllable Loadings and the Impact of Surface Coverage on Catalysis. *J. Am. Chem. Soc.* **2012**, *134*, 2750–2759.
- (15) Terry, T. J.; Stack, T. D. P. Covalent Heterogenization of a Discrete Mn(II) Bis-Phen Complex by a Metal-Template/Metal-Exchange Method: An Epoxidation Catalyst with Enhanced Reactivity. *J. Am. Chem. Soc.* **2008**, *130*, 4945–4953.
- (16) Rimola, A.; Costa, D.; Sodupe, M.; Lambert, J.-F.; Ugliengo, P. Silica Surface Features and Their Role in the Adsorption of Biomolecules: Computational Modeling and Experiments. *Chem. Rev.* **2013**, *113*, 4216–4313.
- (17) Huang, S.; Yang, P.; Cheng, Z.; Li, C.; Fan, Y.; Kong, D.; Lin, J. Synthesis and Characterization of Magnetic Fe₃O₄@SBA-15 Composites with Different Morphologies for Controlled Drug Release and Targeting. *J. Phys. Chem. C* **2008**, *112*, 7130–7137.
- (18) Yang, P.; Huang, S.; Kong, D.; Lin, J.; Fu, H. Luminescence Functionalization of SBA-15 by YVO₄:Eu³⁺ as a Novel Drug Delivery System. *Inorg. Chem.* **2007**, *46*, 3203–3211.
- (19) Reichhardt, N.; Kjellman, T.; Sakeye, M.; Paulsen, F.; Smått, J.-H.; Lindén, M.; Alfredsson, V. Removal of Intra-wall Pores in SBA-15 by Selective Modification. *Chem. Mater.* **2011**, *23*, 3400–3403.
- (20) Kjellman, T.; Reichhardt, N.; Sakeye, M.; Smått, J.-H.; Lindén, M.; Alfredsson, V. Independent Fine-Tuning of the Intra-wall Porosity and Primary Mesoporosity of SBA-15. *Chem. Mater.* **2013**, *25*, 1989–1997.
- (21) Bass, J.; Katz, A. Bifunctional Surface Imprinting of Silica: Thermolytic Synthesis and Characterization of Discrete Thiol–Amine Functional Group Pairs. *Chem. Mater.* **2006**, *18*, 1611–1620.
- (22) Hicks, J.; Jones, C. W. Controlling the Density of Amine Sites on Silica Surfaces Using Benzyl Spacers. *Langmuir* **2006**, *22*, 2676–2681.
- (23) McKittrick, M. W.; Jones, C. W. Toward Single-Site Functional Materials—Preparation of Amine-Functionalized Surfaces Exhibiting Site-Isolated Behavior. *Chem. Mater.* **2003**, *15*, 1132–1139.
- (24) Bass, J. D.; Solovyov, A.; Pascall, A. J.; Katz, A. Acid-Base Bifunctional and Dielectric Outer-Sphere Effects in Heterogeneous Catalysis: A Comparative Investigation of Model Primary Amine Catalysts. *J. Am. Chem. Soc.* **2006**, *128*, 3737–3747.
- (25) Brunelli, N. A.; Venkatasubbaiah, K.; Jones, C. W. Cooperative Catalysis with Acid-Base Bifunctional Mesoporous Silica: Impact of Grafting and Co-condensation Synthesis Methods on Material Structure and Catalytic Properties. *Chem. Mater.* **2012**, *24*, 2433–2442.
- (26) Stein, A.; Melde, B. J.; Schröden, R. C. Hybrid Inorganic-organic Meso-porous Silicates—Nanoscopic Reactors Coming of Age. *Adv. Mater.* **2000**, *12*, 1403–1419.
- (27) Lim, M. H.; Blanford, C. F.; Stein, A. Synthesis of Ordered Microporous Silicates with Organosulfur Surface Groups and Their Applications as Solid Acid Catalysts. *Chem. Mater.* **1998**, *10*, 467–470.
- (28) Wight, A. P.; Davis, M. E. Design and Preparation of Organic–Inorganic Hybrid Catalysts. *Chem. Rev.* **2002**, *102*, 3589–3614.
- (29) Burkett, S. L.; Sims, S. D.; Mann, S. Synthesis of Hybrid Inorganic-organic Mesoporous Silica by Co-condensation of Siloxane and Organosiloxane Precursors. *Chem. Commun.* **1996**, 1367–1368.
- (30) Crisci, A.; Tucker, M.; Lee, M.; Jang, S.; Dumesic, J.; Scott, S. L. Acid-Functionalized SBA-15-Type Silica Catalysts for Carbohydrate Dehydration. *ACS Catal.* **2011**, *1*, 719–728.
- (31) Solin, N.; Han, L.; Che, S.; Terasaki, O. An Amphoteric Mesoporous Silica Catalyzed Aldol Reaction. *Catal. Commun.* **2009**, *10*, 1386–1389.
- (32) Zeidan, R.; Davis, M. E. The effect of acid-base pairing on catalysis: An Efficient Acid-Base Functionalized Catalyst for Aldol Condensation. *J. Catal.* **2007**, *247*, 379–382.
- (33) Zeidan, R. K.; Hwang, S.-J.; Davis, M. E. Multifunctional heterogeneous catalysts: SBA-15-containing Primary Amines and Sulfonic Acids. *Angew. Chem., Int. Ed.* **2006**, *45*, 6332–6335.
- (34) Patel, S. V.; Mlsna, T. E.; Frühberger, B.; Klaassen, E.; Cemalovic, S.; Basel, D. R. Chemically Capacitive Microsensors for Volatile Organic Compound Detection. *Sens. Actuators, B* **2003**, *96*, 541–553.
- (35) Ueno, Y.; Horiuchi, T.; Morimoto, T.; Niwa, O. Microfluidic Device for Airborne BTEX Detection. *Anal. Chem.* **2001**, *73*, 4688–4693.
- (36) Ablat, H.; Yimit, A.; Mahmut, M.; Itoh, K. Nafion Film/K(+)-Exchanged Glass Optical Waveguide Sensor for BTX Detection. *Anal. Chem.* **2008**, *80*, 7678–7683.
- (37) Matsuguchi, M.; Uno, T.; Aoki, T.; Yoshida, M. Chemically Modified Copolymer Coatings for Mass-Sensitive Toluene Vapor Sensors. *Sens. Actuators, B* **2008**, *131*, 652–659.
- (38) Kreuer, K.-D. Proton Conductivity: Materials and Applications. *Chem. Mater.* **1996**, *8*, 610–641.
- (39) Kreuer, K.-D.; Paddison, S. J.; Spohr, E.; Schuster, M. Transport in Proton Conductors for Fuel-Cell Applications: Simulations, Elementary Reactions, and Phenomenology. *Chem. Rev.* **2004**, *104*, 4637–4678.
- (40) Fujita, S.; Kamazawa, K.; Yamamoto, S.; Tyagi, M.; Araki, T.; Sugiyama, J.; Hasegawa, N.; Kawasumi, M. Proton Conductivity under Dry Conditions for Mesoporous Silica with Highly Dense Sulfonic Acid Groups. *J. Phys. Chem. C* **2013**, *117*, 8727–8736.
- (41) Schuster, M.; de Araujo, C. C.; Atanasov, V.; Andersen, H. T.; Kreuer, K.-D.; Maier, J. Highly Sulfonated Poly(phenylene sulfone): Preparation and Stability Issues. *Macromolecules* **2009**, *42*, 3129–3137.
- (42) Schuster, M.; Kreuer, K.-D.; Andersen, H. T.; Maier, J. Sulfonated Poly(phenylene sulfone) Polymers as Hydrolytically and Thermooxidatively Stable Proton Conducting Ionomers. *Macromolecules* **2007**, *40*, 598–607.
- (43) Marschall, R.; Rathouský, J.; Wark, M. Ordered Functionalized Silica Materials with High Proton Conductivity. *Chem. Mater.* **2007**, *19*, 6401–6407.
- (44) Sharifi, M.; Marschall, R.; Wilhelm, M.; Wallacher, D.; Wark, M. Detection of Homogeneous Distribution of Functional Groups in Mesoporous Silica by Small Angle Neutron Scattering and in Situ Adsorption of Nitrogen or Water. *Langmuir* **2011**, *27*, 5516–5522.
- (45) Sharifi, M.; Wallacher, D.; Wark, M. Distribution of Functional Groups in Periodic Mesoporous Organosilica Materials Studied by Small-Angle Neutron Scattering With in situ Adsorption of Nitrogen. *Beilstein J. Nanotechnol.* **2012**, *3*, 428–437.
- (46) Singer, J. A.; Purcell, W. P.; Thompson, C. C. Structure and Properties of Sulfones. I. Electric Moment of 4,4'-diaminodiphenyl Sulfone. *J. Med. Chem.* **1967**, *10*, 528–529.
- (47) Yang, C.; Zibrowius, B.; Schüth, F. A Novel Synthetic Route for Negatively Charged Ordered Mesoporous Silica SBA-15. *Chem. Commun.* **2003**, 1772–1773.
- (48) Yang, C.; Wang, Y.; Zibrowius, B.; Schüth, F. Formation of Cyanide-Functionalized SBA-15 and Its Transformation to Carboxylate-Functionalized SBA-15. *Phys. Chem. Chem. Phys.* **2004**, *6*, 2461–2467.
- (49) Yuan, L.; Tang, Q.; Yang, D.; Zhang, J.-Z.; Zhang, F.; Hu, J. Preparation of pH-Responsive Mesoporous Silica Nanoparticles and

Their Application in Controlled Drug Delivery. *J. Phys. Chem. C* **2011**, *115*, 9926–9932.

(50) Brunauer, S.; Emmett, P. H.; Teller, E. Adsorption of Gases in Multimolecular Layers. *J. Am. Chem. Soc.* **1938**, *60*, 309–319.

(51) Barrett, E. P.; Joyner, L. G.; Halenda, P. P. The Determination of Pore Volume and Area Distributions in Porous Substances. I. Computations from Nitrogen Isotherms. *J. Am. Chem. Soc.* **1951**, *73*, 373–380.

(52) Zhu, Y.; Yuan, H.; Xu, J.; Xu, P.; Pan, Q. Highly Stable and Sensitive Humidity Sensors Based on Quartz Crystal Microbalance Coated with Hexagonal Lamelliform Monodisperse Mesoporous Silica SBA-15 Thin Film. *Sens. Actuators, B* **2010**, *144*, 164–169.

(53) Sauerbrey, G. The Use of Quartz Oscillators for Weighing Thin Layers and for Microweighing. *Z. Phys.* **1959**, *155*, 206–222.

(54) Nyquist, H. Regeneration theory. *Bell. Syst. Technol. J.* **1932**, *11*, 126–147.

(55) Li, Y. J.; Yan, B. Lanthanide (Eu^{3+} , Tb^{3+})/ β -Diketone Modified Mesoporous SBA-15/Organic Polymer Hybrids: Chemically Bonded Construction, Physical Characterization, and Photophysical Properties. *Inorg. Chem.* **2009**, *48*, 8276–8285.

(56) Sun, L. N.; Yu, J. B.; Zhang, H. J.; Meng, Q. G.; Ma, E.; Peng, C. Y.; Yang, K. Y. Near-Infrared Luminescent Mesoporous Materials Covalently Bonded with Ternary Lanthanide [Er(III) , Nd(III) , Yb(III) , Sm(III) , Pr(III)] Complexes. *Microporous Mesoporous Mater.* **2007**, *98*, 156–165.

(57) Sing, K. S. W.; Everett, D. H.; Haul, R. A. W.; Moscou, L.; Pierotti, R. A.; Rouquerol, J.; Siemieniewska, T. Reporting Physisorption Data for Gas/Solid Systems with Special Reference to the Determination of Surface Area and Porosity. *Pure Appl. Chem.* **1985**, *57*, 603–619.

(58) Landau, M. V.; Dafa, E.; Kaliya, M. K.; Sen, T.; Herskowitz, M. Mesoporous Alumina Catalytic Material Prepared by Grafting Wide-Pore MCM-41 With an Alumina Multilayer. *Microporous Mesoporous Mater.* **2001**, *49*, 65–81.

(59) Brinker, C. J.; Scherer, G. W. *Sol-Gel Science*; Academic Press: San Diego, CA, 1990.

(60) Dickert, F. L.; Balumler, U. P. A.; Stathopoulos, H. Mass-Sensitive Solvent Vapor Detection with Calix[4] Resorcinarenes: Tuning Sensitivity and Predicting Sensor Effects. *Anal. Chem.* **1997**, *69*, 1000–1005.

(61) Kundu, T.; Sahoo, S. C.; Banerjee, R. Alkali earth metal (Ca, Sr, Ba) based thermostable metal–organic frameworks (MOFs) for proton conduction. *Chem. Commun.* **2012**, *48*, 4998–5000.

(62) Ōkawa, H.; Sadakiyo, M.; Yamada, T.; Maesato, M.; Ohba, M.; Kitagawa, H. Proton-Conductive Magnetic Metal–Organic Frameworks, $\{\text{NR}_3(\text{CH}_2\text{COOH})\}[\text{M}_a^{\text{II}}\text{M}_b^{\text{III}}(\text{ox})_3]$: Effect of Carboxyl Residue upon Proton Conduction. *J. Am. Chem. Soc.* **2013**, *135*, 2256–2262.

(63) Marschall, R.; Tölle, P.; Cavalcanti, W. L.; Wilhelm, M.; Köhler, C.; Frauenheim, T.; Wark, M. Detailed Simulation and Characterization of Highly Proton Conducting Sulfonic Acid Functionalized Mesoporous Materials under Dry and Humidified Conditions. *J. Phys. Chem. C* **2009**, *113*, 19218–19227.

(64) Van Grotthuss, C. J. D. Sur la Décomposition de l'eau et des Corps Qu'elle Tient en Dissolution à l'aide de l'électricité Galvanique. *Ann. Chim.* **1806**, *58*, 54–73.

(65) Kreuer, K. D.; Weppner, W.; Rabenau, A. Vehicle Mechanism, A New Model for the Interpretation of the Conductivity of Fast Proton Conductors. *Angew. Chem., Int. Ed. Engl.* **1982**, *21*, 208–209.